ARE NATURAL IMAGES OF BOUNDED VARIATION?

YANN GOUSSEAU, JEAN-MICHEL MOREL

Abstract.
The bounded variation assumption is the starting point of many methods in image analysis and processing. However, one common drawback of these methods is their inability to handle textures and small structures properly. We here precisely show why natural images are incompletely represented by BV functions. Through an experimental study of the distribution of bilevels of natural images, we show that their total variation blows up to infinity with the increasing of resolution. To reach these conclusions, we compute bounds on the total variation, and model convolution and sampling under quite general assumptions.

This paper addresses the question of whether natural images may be represented as functions of bounded variation. The question is of relevance because of the wide use of the space BV in image modeling. Roughly speaking, the space BV is the space of functions whose weak derivative is a measure with finite total variation, and is a straightforward space for images since it contains characteristic functions of simple sets, thus enabling the representation of edges. The BV assumption is the starting point of different approaches in image restoration ([15], [17], [5],[10]), image segmentation ([2]), image deconvolution ([16], [9]), optical flow computation ([4]) or image compression. These methods have proven very efficient, especially in dealing with one dimensional discontinuity in images. However, one common drawback is their inability to handle textures properly. In particular, restoration or deconvolution in BV leads to the smoothing out of textures, and segmentation procedures in BV fail to isolate textured area. A recent paper ([13]) yields mathematical proofs of the staircasing effect, according to which BV-minimization tends to create constant patches in images, thus eliminating textural effects.

In this paper, we show that this phenomenon can be explained by the fact that natural images are not of bounded variation. Our approach combines an experimental program we performed on the distribution of homogeneous and connected regions in images, the sections, and a theoretical result bounding from below the BV norm of two-dimensional functions according to the distribution of their sections. We formalize the link between experiments on discrete images and the mathematical results by using a simple model of convolution and sampling for the formation of numerical images. We here point out that another method to estimate the BV norm of images relies on the study of wavelet coefficients. In order to study locally the (ir)regularity of a signal one may investigate the decay of wavelet coefficients at a certain location (see [12], [11] for an introduction to wavelet decompositions). More recently, the link between the global decay of wavelet coefficients and the BV norm has been studied, so that, in some cases, this decay permits to decide whether or not a function belongs to the space BV, see [6], [14]. We shall compare our method and the wavelet method to decide whether an image is in BV or not. As we shall see, the geometric measurements we perform seem more accurate and permit to show that natural images are not of bounded variation.

The paper is organized as follows: in Section 1, we recall our results about the power law distribution of sections area and perimeter. In Section 2, we recall basic

*CMLA, ENS Cachan
61 av. du Président Wilson, 94235 Cachan Cedex, France.

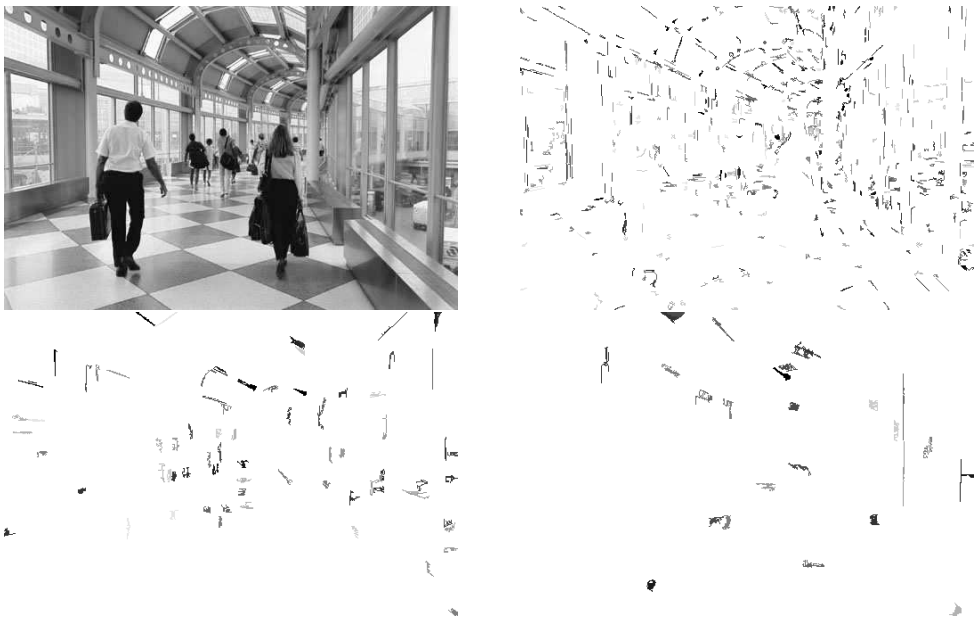

FIG. 1. *airport, 510 × 343 image, with some of its sections for* $k = 10$. *Top right sections are of size between 10 and 20 pixels; bottom left between 40 and 50 pixels;bottom right between 80 and 90 pixels. Different gray levels correspond to sections from different k-bilevels*

definitions and properties related to the space BV of functions with bounded variation. In Section 3, we establish a link between the distribution of sections size and the BV norm of functions of $\mathbb{R}^2$; in Section 4, we show that by combining the experimental results of Section 1 and the theoretical results of Section 3, we can conclude that natural images are not of bounded variation. Eventually, in Section 5, we compare our conclusions with recent results on the decay of wavelet coefficients.

1. The distribution of bilevels in natural images. In previous papers, see [1], [8], we explored the statistics of homogeneous and connected regions of natural images. The most remarkable fact is that the distributions of their area and perimeter are very well approximated by a power law. More precisely, we consider a digital image I, whose gray levels are between 0 and N. For an integer k, we call a k-bilevel of I any of the binary images defined by

$$I_l(i,j) = \begin{cases} 1 & \text{if } I(i,j) \in \left[(l-1)\frac{N}{k}, l\frac{N}{k}\right), \\ 0 & \text{otherwise,} \end{cases}$$

for l varying from 1 to k. We then define a section to be a connected component of a set $\{(i,j)/I_l(i,j) = 1\}$, for some l. For each integer a, we define $f(a)$ to be the number of sections with area a (in pixels). Our experiments show that

$$f(a) \approx \frac{C}{a^\alpha}, \tag{1.1}$$

where C and α are image dependent constants. Moreover, in most images, α is close to 2.

We will not recall here all the experimental results, and we refer to the previously mentioned papers for more details, but we will give some examples. For each image,

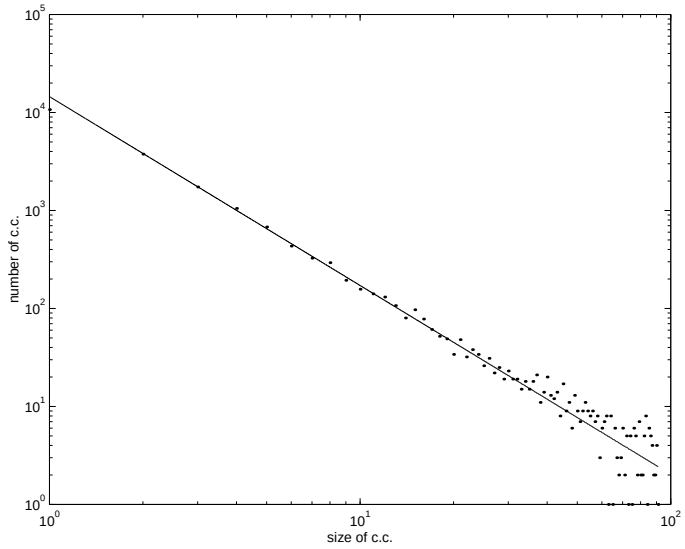

FIG. 2. *Function f (section area distribution) for the airport image, Figure 1, in log-log coordinates.*

we fit a straight line with slope α to the function f in log-log coordinate, minimizing the least squares distance. We also compute the least squares error E. In Figure 1, we display a digital image and some of its sections, and in Figure 2 the corresponding fit for f. Similar graphics are obtained for all considered digital images (either from a digital camera, scanned, or calibrated images). In Table 1, we display results averaged over hundred calibrated images from a database collected by van Hateren, freely available at http://hlab.phys.rug.nl/imlib/, see [18]. The most noticeable fact here is the proximity of α to 2, and the fact that for all images and some value of k, α is larger than 1.5, fact that will be proven relevant in the following for estimating the BV norm of images.

In [1], [8], we also studied the distribution of the perimeters of sections, which are also distributed according to a power law, with an exponent β usually between 2 and 3. In Table 2, we display results similar to those in Table 1 for the values of β (still computed by minimizing the least squares error in log-log coordinates) on the previously mentioned images database.

Are small sections due to noise or microtextures ? In Figure 1, we have shown some of the small sections from which the size statistics are estimated. We do that for the following purpose : it might be objected to the observed size laws that their small scale behaviour is due to the caption device and not to the underlying "natural" image. Thus, it is very relevant to look at the sections and decide whether they are due to digitization noise, to some microtexture, or to the inherent geometric structure of the image. In Figure 1, we can check that most small sections arise on contrasted parts of the image (the so called "edges") and that their shape coincides with those edges. We can also rule out a Gibbs phenomenon : It multiplies the edge contribution to the BV norm by a fixed constant factor. We have only shown one example, but we have chosen a kind of example for which the BV model should be very likely, since the whole scene is a geometric human made scene, with as little texture as possible. All other images we have checked confirm this interpretation :

TABLE 1

Average results for the distribution of area of sections on 100 images from the van Hateren database. We denote by $< \alpha >$ and $< E >$ the mean values of α and E respectively; std α the standard deviation of α; min(α) and max(α) the minimum and maximum values for α.

k	$< \alpha >$	std α	max α	min α	$< E >$	max E
16	1.85	0.19	2.20	1.39	0.37	0.49
14	1.83	0.19	2.18	1.36	0.37	0.54
12	1.83	0.19	2.15	1.37	0.37	0.54
10	1.81	0.18	2.12	1.27	0.37	0.50
8	1.80	0.17	2.26	1.32	0.38	0.59

TABLE 2

Average results for the distribution of perimeter of sections on 100 images from the van Hateren database. Notations are the same as for Table 1.

k	$< \beta >$	std β	max β	min β	$< E >$	max E
16	2.35	0.28	2.57	2.04	0.36	0.42
14	2.42	0.29	2.60	2.10	0.29	0.35
12	2.38	0.33	2.63	1.99	0.42	0.51
10	2.46	0.15	2.62	2.10	0.31	0.39
8	2.36	0.14	2.49	2.04	0.37	0.41

small sections correspond to objects or pieces of objects, or pieces of contours. They are not at all uniformly distributed over the image, as would happen with noise.

2. Functions of bounded variation and sets of finite perimeter. In this section, we recall some basic facts about functions of bounded variation. Let I be a bounded function defined on a domain (e.g. rectangular) $\Omega \subset \mathbb{R}^2$. I is in $BV(\Omega)$, the space of function with bounded variations, if

$$||I||_{BV} \stackrel{\text{def}}{=} \int_\Omega |DI| < +\infty,$$

where the gradient DI is to be understood in a weak sense (see [19]):

$$\int_\Omega |DI| = \sup \left\{ \int_\Omega I \text{div}\phi \mid \phi \in C_c^1(\Omega), |\phi| < 1 \right\},$$

where $C_c^1(\Omega)$ is the space of continuously differentiable functions with compact support, defined from Ω to $\mathbb{R}^2$. Actually the usual BV norm is defined as the sum of $\int |DI|$, the total variation, and the L^1 norm, $\int |I|$. We only consider here the total variation (which is not a norm), and write it $||.||_{BV}$.

We will be interested in a more geometric characterization of $BV(\Omega)$. For $\lambda \in \mathbb{R}$, define the level set of I with level λ by

$$\chi_\lambda I = \{x, I(x) \geq \lambda\}.$$

Now (see [7]) recall that a set $E \in \Omega$ is of finite perimeter per(E) if

$$\text{per}(E) \stackrel{\text{def}}{=} ||\mathbb{1}_E||_{BV} \leq +\infty,$$

where $\mathbb{1}_E$ is the characteristic function of the set E. This definition generalizes the usual definition of the boundary length, in the sense that both definitions are equivalent in the case of a set with piecewise regular boundary. If a function has

bounded variation then, for almost every $\lambda \in \mathbb{R}$, $\chi_\lambda I$ is a set with finite perimeter and (coarea formula, see [7]),

$$||I||_{BV} = \int_{\mathbb{R}} \mathrm{per}(\chi_\lambda I) d\lambda. \tag{2.1}$$

Conversely, if $\mathrm{per}(\chi_\lambda I)$ is finite (for almost all λ) and the preceding integral is finite, then I has bounded variation. We also recall that, by the classical isoperimetric inequality, we have for every set O with finite perimeter,

$$\mathrm{per}(O) \geq 2\pi^{\frac{1}{2}} \nu(O)^{\frac{1}{2}}, \tag{2.2}$$

where $\nu(O)$ denotes the Lebesgue measure of O.

The BV space is a very straightforward space for images. First, if images are neither continuous nor strictly differentiable, it seems reasonable to assume them to be in a space where they are weakly differentiable. Moreover, the occlusion phenomenon is responsible for one-dimensional discontinuities which prevent the weak derivatives of images to be integrable, thus forcing images out of any Sobolev space. Such a simple image as a white disk on a black background belongs to the space BV, which is the natural space to perform calculus of variations on functions whose one-dimensional discontinuities have finite length (see [2]). Now, a first way for an image not to be in this space is to have level lines with infinite length. For instance, the characteristic functions of two-dimensional sets with fractal boundaries will not be of bounded variation. There is also another way for a function not to be in BV. Each of its level lines may be of finite perimeter, while the sum of these level lines' perimeters is infinite. As we will see in the next two sections, this is what happens for natural images, in which, in a precise sense, small objects are too numerous for the function to be of bounded variation.

3. A lower bound for the BV norm. In the following, we shall consider sections of the image. We always assume that the image I satisfies $0 \leq I(x) \leq C$. We first fix two parameters γ, λ, with $0 \leq \lambda \leq \gamma$. For any $n \in \mathbb{N}$, we consider the bilevel sets of I

$$\{x, \lambda + (n-1)\gamma \leq I(x) < \lambda + n\gamma\} = \chi_{\lambda+(n-1)\gamma} I \setminus \chi_{\lambda+n\gamma} I.$$

We call (γ, λ)-section of I any set which is a connected component of a bilevel set $\chi_{\lambda+(n-1)\gamma} I \setminus \chi_{\lambda+n\gamma} I$ for some n. We denote each one of the components by $S_{\gamma,\lambda,i}$ for $i \in J(\gamma, \lambda)$, a set of indices. Notice that the (γ, λ)-sections are disjoint and their union is the image domain Ω,

$$\bigcup_{i \in J(\gamma,\lambda)} S_{\gamma,\lambda,i} = \Omega. \tag{3.1}$$

There are several ways to define the connected components of a set with finite perimeter, since such a set is defined up to a set with zero Lebesgue measure. One can prove ([3]) that a definition of connected components for a set with finite perimeter permits the following statements (recall that ν is the 2-dimensional Lebesgue measure and per is the perimeter):

DEFINITION 3.1. *Let X be a set with finite perimeter in $\mathbb{R}^2$. We say that X is not decomposable if we cannot write it as $X = Y \cup Z$, with $\nu(Y) > 0$, $\nu(Z) > 0$, $\nu(X) = \nu(Y) + \nu(Z)$ and $per(X) = per(Y) + per(Z)$.*

THEOREM 3.2. *Each set of finite perimeter X admits a unique decomposition*

$$X = \cup_n X_n,$$

where the union is finite or countable, and such that
(i) each X_n is not decomposable,
(ii) for each n, $\nu(X_n) > 0$,
(iii) $per(X) = \sum_n per(X_n)$.

This definition matches the usual requirements of connectivity, in particular, if for $x \in X$, cc(x,X) is the component relative to X that contains x, $X \subset Y$ implies $cc(x, X) \subset cc(x, Y)$.

We need this definition because (iii) will enable us to use the distribution of sections, as experimentally observed in Section 1, to bound the BV norm of images from below. We denote by $J(n) \subset J(\gamma, \lambda)$ the set of indices of sections which are connected components of $\chi_{\lambda+(n-1)\gamma} I \setminus \chi_{\lambda+n\gamma} I$. Note that by classical results on BV functions, for each γ, $\chi_{\lambda+(n-1)\gamma} I \setminus \chi_{\lambda+n\gamma} I$ has finite perimeter for almost every λ. As an obvious consequence of Proposition 3.2, we have

COROLLARY 3.3. *Let I belongs to BV. Then for almost every λ,*

$$per(\chi_{\lambda+(n-1)\gamma} I \setminus \chi_{\lambda+n\gamma} I) = \sum_{i \in J(n)} per(S_{\lambda,\gamma,i}).$$

In order to estimate the BV norm of I, we shall need

LEMMA 3.4. *If $B \subset A$ are two sets with finite perimeter, then*

$$per(A \setminus B) \leq per(A) + per(B).$$

Proof. Recall that $\mathrm{per}(A) = ||\mathbb{1}_A||_{BV}$. Then by the subadditivity of the BV norm, we deduce from

$$\mathbb{1}_{A \setminus B} = \mathbb{1}_A - \mathbb{1}_B$$

that

$$\mathrm{per}(A \setminus B) \leq \mathrm{per}(A) + \mathrm{per}(B).$$

□

In the following theorem, we analyze the statistics of sizes of sections as follows. We fix γ, that is, the overall contrast of considered sections and for each $0 \leq \lambda \leq \gamma$, we count all sections $S_{\gamma,\lambda,i}$ which have an area between s_1 and s_2, with $0 < s_1 < s_2$. That is to say we consider the integer

$$\mathrm{Card}\{i, s_1 \leq \nu(S_{\gamma,\lambda,i}) < s_2\}.$$

Note that this number is bounded since Ω is bounded and the sections are disjoint. We average this number over all λ's in $[0, \gamma]$, to obtain the function

$$f(\gamma, s_1, s_2) = \int_0^\gamma \mathrm{Card}\{i, s_1 \leq |S_{\gamma,\lambda,i}| < s_2\} d\lambda$$

Remark: To be able to define f, we made the assumption that

$$\mathrm{Card}\{i, s_1 \leq \nu(S_{\gamma,\lambda,i}) < s_2\} \text{ is a measurable function of } \lambda \tag{3.2}$$

We will suppose that for some $\gamma > 0$, this average number has a density $f(\gamma, s)$ with respect to s. That is:

$$\forall s > 0 \qquad \lim_{s_1 \uparrow s, s_2 \downarrow s} \frac{f(\gamma, s_1, s_2)}{s_1 - s_2} = f(\gamma, s). \tag{3.3}$$

Then we have the following bound for the BV norm of I:

THEOREM 3.5. *Let I be in $BV(\Omega)$. Assume that there exists some $\gamma > 0$ such that (3.2) and (3.3) hold (i.e. the average number of sections with area s, for $0 \leq \lambda \leq \gamma$, has a density $f(\gamma, s)$), then*

$$||I||_{BV} \geq \pi^{\frac{1}{2}} \int_0^{\nu(\Omega)} s^{\frac{1}{2}} f(\gamma, s) ds. \tag{3.4}$$

Proof. Applying Corollary 3.3 and Lemma 3.4,

$$\begin{aligned}
||I||_{BV} &= \int_{\mathbb{R}} \mathrm{per}\{x, I(x) \geq \lambda\} d\lambda \\
&= \frac{1}{2} \left(\int_{\mathbb{R}} \mathrm{per}\{x, I(x) \geq \lambda\} d\lambda + \int_{\mathbb{R}} \mathrm{per}\{x, I(x) \geq \lambda - \gamma\} d\lambda \right) \\
&\geq \frac{1}{2} \int_{\mathbb{R}} \mathrm{per}(\chi_{\lambda-\gamma} I \setminus \chi_\lambda I) d\lambda \\
&= \frac{1}{2} \sum_{n \in \mathbb{Z}} \int_{n\gamma}^{(n+1)\gamma} \mathrm{per}(\chi_{\lambda-\gamma} I \setminus \chi_\lambda I) d\lambda \\
&= \frac{1}{2} \int_0^{\gamma} \sum_{n \in \mathbb{Z}} \mathrm{per}(\chi_{\lambda+(n-1)\gamma} I \setminus \chi_{\lambda+n\gamma} I) d\lambda \\
&= \frac{1}{2} \int_0^{\gamma} \sum_{i \in J(\gamma,\lambda)} \mathrm{per}(S_{\gamma,\lambda,i}) d\lambda.
\end{aligned}$$

By the isoperimetric inequality (2.2), we therefore obtain

$$||I||_{BV} \geq \pi^{\frac{1}{2}} \int_0^{\gamma} \sum_{i \in J(\gamma,\lambda)} \nu(S_{\gamma,\lambda,i})^{\frac{1}{2}} d\lambda.$$

Then, for any $n \in \mathbb{N}^*$

$$||I||_{BV} \geq \pi^{\frac{1}{2}} \sum_{k=1}^{n-1} \left(\frac{\nu(\Omega)}{n} k \right)^{\frac{1}{2}} f\left(\gamma, \frac{\nu(\Omega)}{n} k, \frac{\nu(\Omega)}{n} (k+1) \right). \tag{3.5}$$

We introduce the functions

$$f_n = \sum_{k=1}^{n-1} \left(\frac{\nu(\Omega)}{n} k \right)^{\frac{1}{2}} f\left(\gamma, \frac{\nu(\Omega)}{n} k, \frac{\nu(\Omega)}{n} (k+1) \right) \frac{n}{\nu(\Omega)} \mathbb{1}_{\left[\frac{\nu(\Omega)}{n} k, \frac{\nu(\Omega)}{n}(k+1)\right)}.$$

We have

$$||I||_{BV} \geq \pi^{\frac{1}{2}} \int_0^{\nu(\Omega)} f_n(s) ds,$$

and

$$\forall s_0 > 0 \qquad f_n(s_0) \underset{n\to+\infty}{\longrightarrow} (s_0)^{\frac{1}{2}}\gamma f(\gamma, s_0),$$

thanks to Hypothesis (3.3). Therefore, by Fatou's lemma

$$||I||_{BV} \geq \pi^{\frac{1}{2}} \int_0^{\nu(\Omega)} s^{\frac{1}{2}} f(\gamma, s) ds.$$

□

We can repeat the preceding analysis by assuming now that

$$g(\gamma, p_1, p_2) = \int_0^{\gamma} \text{Card}\{i, p_1 \leq \text{per}(S_{\gamma,\lambda,i}) \leq p_2\} d\lambda$$

has an average density $g(\gamma, p)$ with respect to p (once more assuming the cardinal we integrate is measurable). That is to say

$$\lim_{p_1\uparrow p, p_2\downarrow p} \frac{g(\gamma, p_1, p_2)}{p_2 - p_1} = g(\gamma, p). \tag{3.6}$$

Then we have the analog of Theorem 3.5 for the perimeters of sections:

THEOREM 3.6. *Let I be in $BV(\Omega)$. Assume that there exists some $\gamma > 0$ such that (3.6) holds, i.e. the average number of sections with perimeter s, for $0 \leq \lambda \leq \gamma$, has a density $g(\gamma, p)$. Then*

$$||I||_{BV} \geq \frac{1}{2} \int_0^{+\infty} p g(\gamma, p) dp. \tag{3.7}$$

Proof. In the same way as before (without using the isoperimetric inequality), and fixing some $p_m > 0$

$$\begin{aligned} ||I||_{BV} &\geq \frac{1}{2} \int_0^{\gamma} \sum_{i\in J(\gamma,\lambda)} \text{per}(S_{\gamma,\lambda,i}) d\lambda \\ &\geq \frac{1}{2} \sum_{k=1}^{n-1} \left(\frac{p_m}{n} k\right) g\left(\gamma, \frac{p_m}{n} k, \frac{p_m}{n}(k+1)\right). \end{aligned}$$

As before this implies

$$||I||_{BV} \geq \frac{1}{2} \int_0^{+\infty} p g(\gamma, p) dp.$$

□

4. Application: natural images are not of bounded variation.

4.1. The continuous framework. In this section, we draw the consequences of Theorems 3.5 and 3.6 for the images analyzed in Section 1, by assuming that the observed distribution of sections approximates the distribution in continuous images. According to our experimental results, we suppose that the considered images satisfy

$$f(\gamma, s) = \frac{C}{s^\alpha} \tag{4.1}$$

$$g(\gamma, p) = \frac{C}{p^\beta} \tag{4.2}$$

for some constants $\alpha > 0$, $\beta > 0$, where f is the density for the area distribution of the sections, and g the density for the perimeters. This law has been experimentally checked for several values of $\gamma = \frac{256}{k}$ (the grey level width of the sections), k ranging from 8 to 20, see Section 1 and [8]. We also checked that the value of α was almost unchanged when the bilevels were not defined from gray level 0, but from some gray level less that $\frac{256}{k}$ (that is to say, in the continuous model, for different values of λ), and that when averaging the experimental density function over integer values of λ between 0 and $\gamma = \frac{256}{k}$, f and g still are power laws with the same exponent. Thus, Hypotheses 4.1 and 4.2 are valid. We here emphasized that the shapes and locations of small sections indicate that these are not due to noise, but to small structures and objects clearly present in the image, particularly pieces of edges, see Figure 1. Moreover, Gaussian white noise leads to quite different statistics, see [8].

Then, by Theorem 3.5, we have

$$||I||_{BV} \geq c \int_0^{\nu(\Omega)} \frac{C s^{\frac{1}{2}}}{s^\alpha} ds,$$

and in the same way,

$$||I||_{BV} \geq c \int_0^{+\infty} \frac{Cp}{p^\beta} dp.$$

Thus, if we admit that (4.1) and (4.2) indeed hold for natural images when $s \to 0$, as is indicated by the experiments recalled in Section 1, we obtain that the considered images are not in BV if $\alpha > \frac{3}{2}$, or $\beta > 2$, since the corresponding integrals are not finite. These values of α and β have been checked for all images of the database studied in Section 1, for some value of k, except for some (3 out of 100) blured images. The assumption that Formulae 4.1 and 4.2 hold for small scales, below the scale of pixelisation, is a strong one, but the experiment of Section 1 indicates that the distribution is the same at all scales. Moreover, the next section will analyze the effect of pixelisation on the BV norm. Of course, there exists a cut-off scale in images, but the lower bounds we found for the BV norm indicate that the contribution of small scales to the value of this norm is unexpectedly large compared to the contribution of larger scales. As mentioned in the introduction, this should be related to the problem of the erasing of textures by variational methods minimizing the total variation of images. Indeed, the BV-norm gives a large weight to small scales textures, that are known to disappear in the process of restoration (debluring or denoising for instance) by such variational methods, see [17], [10].

4.2. Convolution and sampling. In this section, we draw the same conclusions as in the previous one about the BV norm of natural images, with a more rigorous interpretation of our experimental results. We give a practical application of the method of Theorem 3.5, in a case where its hypotheses are satisfied. We assume that discrete images, on which we performed the analysis of Section 1, are obtained from continuous ones through convolution and sampling. We first show that when we compute the BV norm of a function after convolution with a rescaled smoothing kernel (under some regularity conditions) and sampling, we underestimate the actual value of the BV norm of the initial function. We write G for a two dimensional function, C for the square whose lower left corner is (0,0), and upper right corner (1,1), n an integer, and for a real number x, $[x]_n = [nx]/n$, $[nx]$ being the integer part of nx.

LEMMA 4.1. *Let I be a function in $BV(C)$, let $G_n(x,y) = G(nx,ny)$, define*

$$I_c = I * G_n,$$

and for $(x,y) \in C$

$$I_n(x,y) = I_c([x]_n + \frac{1}{2n}, [y]_n + \frac{1}{2n}).$$

Assume that there exists some functions a and b such that

$$\forall x, y \in C \qquad |G(x,y)| \leq a(x)b(y) \tag{4.3}$$

and a constant K such that

$$\sup_{x,y} \sum_{i,j} a(x+i)b(y+j) \leq K. \tag{4.4}$$

Then

$$||I_n||_{BV(C)} \leq \sqrt{2}K||I||_{BV(C)}$$

proof. For i, j integer in $[0,n)$, define

$$I_{i,j} = I_c(\frac{i}{n} + \frac{1}{2n}, \frac{j}{n} + \frac{1}{2n}).$$

We have

$$||I_n||_{BV} = \sum_{i,j} \left(|I_{i,j} - I_{i-1,j}| + |I_{i,j} - I_{i,j-1}| \right).$$

Now, for all i, j,

$$\begin{aligned}
|I_{i,j} - I_{i-1,j}| &= \left| \int \left(I(\frac{i+1}{n} - x, \frac{j}{n} - y) - I(\frac{i}{n} - x, \frac{j}{n} - y) \right) G(nx,ny) \right| \\
&= \left| \int \int_0^1 \frac{\partial}{\partial x} I(\frac{i+t}{n} - x, \frac{j}{n} - y) G(nx,ny) \right| \\
&\leq \int \int_0^1 \left| \frac{\partial}{\partial x} I(\frac{i+t}{n} - x, \frac{j}{n} - y) \right| a(nx)b(ny) \\
&\leq \int \int_0^1 \left| \frac{\partial}{\partial x} I(\frac{t}{n} - x, -y) \right| a(nx+i)b(ny+j)
\end{aligned}$$

so that

$$\sum_{i,j} |I_{i+1,j} - I_{i,j}| \leq \sup_{x,y} \sum_{i,j} a(x+i)b(y+j) \int \left| \frac{\partial}{\partial x} I \right|,$$

and thus

$$||I_n||_{BV} \leq K \int \left| \frac{\partial}{\partial x} I \right| + \left| \frac{\partial}{\partial y} I \right| \leq \sqrt{2} K ||I||_{BV},$$

the last inequality resulting from $|u| + |v| \leq \sqrt{2}(u^2 + v^2)^{1/2}$. □

This theorem enables us to reformulate the fact that natural images do not belong to BV in a slightly different way. Suppose that the continuous image I is represented by the discrete function I_n of the previous theorem. Assume moreover that the distribution of the area of the discrete connected components of bilevels for I_n is $f_{n,\gamma}(k)$, for values of k from 1 to n^2. Then reasoning as in Theorem 3.5 leads to

THEOREM 4.2. *Let I be a function in $BV(C)$ and I_n a sampling of I, defined as in Lemma 4.1, the kernel G satisfying Hypotheses (4.3) and (4.4). Then there is a constant C such that*

$$||I||_{BV} \geq C \sum_{k=1}^{n^2} \left(\frac{1}{n^2} k \right)^{\frac{1}{2}} f_n(\gamma, k), \tag{4.5}$$

where $f_n(\gamma, k)$ is the number of connected components of I_n of area k, for values of k from 1 to n^2.

proof. Since I_n is a step function, all measurability conditions of Theorem 3.5 are satisfied, and we obtain Formula (3.5) which yields

$$||I_n||_{BV} \geq C \sum_{k=1}^{n^2} \left(\frac{1}{n^2} k \right)^{\frac{1}{2}} f_n(\gamma, k).$$

By Lemma 4.1, we obtain Formula (4.5). □

We now come to the consequences of our experiments:

COROLLARY 4.3. *If for all n, there is a constant C_n such that*

$$f_n(\gamma, k) \geq \frac{C_n}{\left(\frac{1}{n^2} k\right)^{\alpha}}, \tag{4.6}$$

with $\alpha < 2$, then

$$||I_n||_{BV} \geq C \sum_{k=1}^{n^2} \frac{1}{n^2} \left(\frac{k}{n^2} \right)^{\frac{1}{2} - \alpha}. \tag{4.7}$$

proof. We have (computing the area of the unit square)

$$\sum_{k=1}^{n^2} f_n(\gamma, k) \frac{k}{n^2} = 1,$$

so that

$$C_n \sum_{k=1}^{n^2} \frac{1}{n^2} \left(\frac{k}{n^2} \right)^{1-\alpha} \geq \frac{1}{n^2}.$$

Now if $\alpha < 2$, the preceding Riemann sum converges, and

$$C_n \geq \frac{(2-\alpha)}{n^2}.$$

Eventually, replacing Expression (4.6) into Formula (4.5) yields the result. □

Now the same conclusions as before hold, since the right side of Formula (4.7) tends to infinity as soon as $\alpha > 1.5$. We have thus proved that if the distribution of the (discrete) sections of the (piecewise constant) function which is obtained by convolving I with a rescaled filter and sampling at n^2 points follows Formula (4.6) with $1.5 < \alpha < 2$, then I is not of bounded variation.

Remark: The assumption of Corollary 4.3 correspond exactly to our numerical experiments on natural images. Notice that we observed a variation of the constant C_n, and that the preceding proof shows that the blow up result for the BV norm of images is independent of this variation.

5. Wavelets and the space BV. As mentioned in the introduction, recent results concerning the link between the global decay of wavelet coefficients and the total variation of images permit us to address the main question of this paper in a wavelet framework. Let (c_k) be the wavelets coefficients of the image I, ordered in a non increasing sequence. We say that the c_k's are in l^1 if $\sum |c_k| < +\infty$, and that they are in weak-l^1 if there exists a constant C such that $c_k \leq \frac{C}{k}$. Obviously l^1 is included in weak-l^1. It is well known that if the c_k are in l^1, then I is in a Besov space included in BV. In the other direction, Cohen, DeVore, Petrushev and Xu, [6], recently proved that if I is in BV, then the c_k's are in weak-l^1, for the Haar wavelets. Cohen, Meyer and Oru then generalized the result to any compactly supported wavelet basis, see [14].

Thus, it is possible to decide whether an image belongs or not to BV by looking at its wavelet coefficients decay, except if they decrease as $\frac{C}{k}$, which happens to be the case quite often. We present in Figure 3 the ordered coefficients for four images: the well known Lena image, a part of a baobab image, a baboon image (Figure 4), and a Gaussian white noise. We used Daubechies' wavelets (using filters of length 8 provided by Wavelab), and found very similar results with Haar's wavelets. As we see, there is a fairly linear part in those graphs, but only for intermediate scales. Assuming the small scales behavior is perturbed by sampling, and that the decay observed for most of the coefficients is characteristic of what happens at small scales, we may use the preceding results. We fitted a line to those values according to a least squares error, so that an image should be in BV when the slope of this line is (strictly) greater than 1, and out of BV if the slope is (strictly) smaller than 1. In the case of the baobab and baboon images (Figure 4), we respectively found slopes of 0.76 and 0.45, and values of α (the exponent of the power law distribution of sections area)respectively equals to 1.9 and 2.38 (for $k = 16$), so that both methods agree: those images are not in BV. For the well-known image of Lena, our approach gives an α of 1.9 (for $k = 16$), which suggests Lena being clearly out of BV, whereas from the wavelet approach, a slope of .95 indicates the image is not BV. Now, this result is close to the uncertainty zone. Of course, the decay of the coefficients for the noise image is very slow (0.16) so that this image is not in BV, whereas the distribution of the area of sections does not follow a power law (but an exponential distribution). Note that in all four cases, the inference of the distribution at small scales is less clear than in the morphological approach of the previous sections.

To understand the nature of the uncertainty when the slope is 1, it is worth

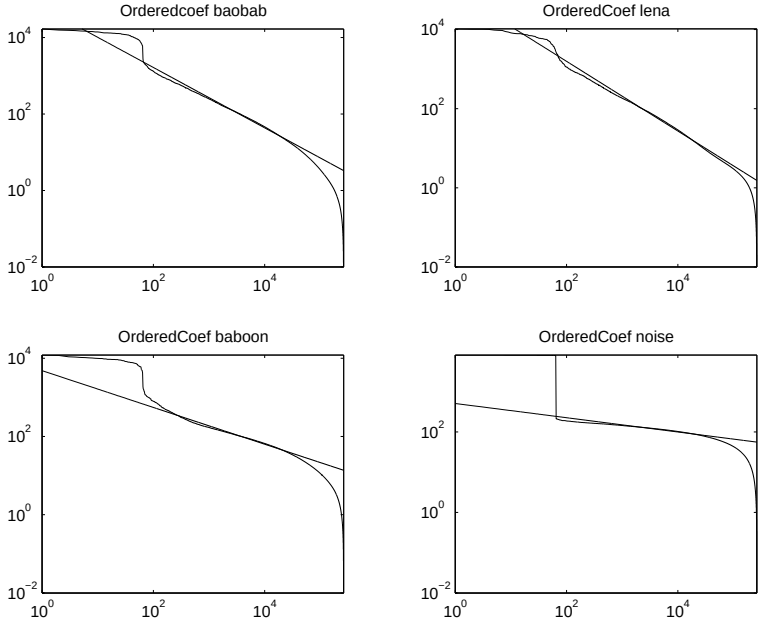

FIG. 3. *Ordered wavelet coefficients (modulus against the rank in log-log coordinates) and least squares fit for four images*

FIG. 4. *Lena, baobab and baboon images, on which we study the decay of wavelet coefficients as shown in Figure 3*

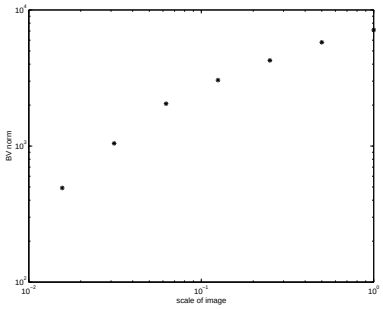

FIG. 5. *Simple plot of the BV norm as a function of the scale, for the image of the airport. The BV norm is directly computed on the image which is successively downsampled. Abscissa equals a half means the image has been subsampled by a factor 2*

noticing that the wavelet coefficients produced by the characteristic function of a simple shape already decrease as $\frac{1}{k}$, so that the simple presence of edges in the image implies this type of decay. In a sense, the wavelet coefficients look at the smoothness of the edges of the image, whereas, by investigating the sections size distribution, we investigate the number and the cumulated length of those sections. Thus, as we mentionned already, it is not surprising that we get more precise estimates of the image oscillations at small scales, and can therefore decide for instance that Lena is not BV while the wavelet coefficient analysis is ambiguous [11].
Clearly, our proposed procedure and the wavelet experiments imply that the scale behaviour of the image needs some sophisticated statistics to be correctly extrapolated at fine scales. Thus, it is necessary to point out that less sophisticated statistics can yield uninterpretable results on images for which the former mentionned methods yield clearcut answers. By one of the referee's suggestions, we performed the following experiment (Figure 5). We simulated a zoom backward at six dyadic scales of a natural image and computed the resulting BV norm. In several images were the section statistics is conclusive, we get no clear scaling behaviour, as can be seen in Figure 5. Actually, even if the dots in the just mentionned experiment had been aligned, we could'nt have made any strong statement. The number of obtainable samples is simply too small.

6. Conclusion. Combining experimental results about the distribution of sections in natural images and a result about the total variation of functions of $\mathbb{R}^2$, we have shown that natural images are not of bounded variation. This conclusion relies on the assumption that the observed images are obtained from continuous ones through fairly arbitrary convolution and sampling. This shows precisely that even if well adapted to the large scale geometric structures of images, modeling them as functions with bounded variation does not account for the intricate nature of their small details.

REFERENCES

[1] L. Alvarez, Y. Gousseau, and J.-M. Morel, *The size of objects in natural and artificial images*, Advances in Imaging and Electron Physics, Academic Press, 111 (1999), pp. 167–242.
[2] L. Ambrosio, *Variational problems in SBV*, Acta Applicandae Mathematicae, 17 (1989), pp. 1–40.
[3] L. Ambrosio, V. Caselles, S. Masnou, and J.-M. Morel, *Connected components of sets of finite perimeter and applications to image processing*, Journal of the European Mathematical Society, 3 (2001), pp. 39–92.
[4] G. Aubert, R. Deriche, and P. Kornprobst, *Computing optical flows via variational techniques*, SIAM Journal on Applied Mathematics, 60 (1999), pp. 156–182.
[5] T. Chan and C. Wong, *Total variation blind deconvolution*, IEEE Transactions on Image Processing, 7 (1998), pp. 370–375.
[6] A. Cohen, R. DeVore, P. Petrushev, and H. Xu, *Non linear approximation and the space $BV(\mathbb{R}^2)$.*, Amer. J. Math., 121 (1999), pp. 587–628.
[7] L. C. Evans and R. F. Gariepy, *Measure Theory and Fine Properties of Functions.*, Studies in Advanced Math., CRC Press, 1992.
[8] Y. Gousseau, *La distribution des formes dans les images naturelles*, PhD thesis, CEREMADE, Université Paris IX, Janvier 2000.
[9] J. Kalifa, S. Mallat, and B. Rougé, *Minimax deconvolution in mirror wavelet bases.* Submitted to *IEEE Trans. on Image Processing*, 1999.
[10] F. Malgouyre, *Spectrum interpolation and image deblurring by means of the total variation.* Submitted to *IEEE Trans. on Image Processing*, 1999.
[11] S. Mallat, *A Wavelet Tour of Signal Processing*, Academic Press, 2nd ed., 1999.
[12] Y. Meyer, *Wavelets: Algorithms and Applications*, SIAM, 1993.

[13] M. NIKOLOVA, *Local strong homogeneity of a regularized estimator*, Int'l Journal of Computer Vision, 61 (2000), pp. 633–658.
[14] F. ORU, *Rôle des oscillations dans quelques problèmes d'analyse non-linéaire*, PhD thesis, ENS Cachan, 1998.
[15] L. RUDIN, *Images, Numerical Analysis of Singularities and Shock Filters*, PhD thesis, California Institute of Technology, 1987.
[16] L. RUDIN AND S. OSHER, *Total variation based image restoration with free local constraints*, in IEEE ICIP, vol. 1, Austin, Texas, 1994, pp. 31–35.
[17] L. RUDIN, S. OSHER, AND E. FATEMI, *Nonlinear total variation based noise removal algorithms.*, Physica D, 60 (1992), pp. 259–268.
[18] J. VAN HATEREN AND A. VAN DER SCHAAF, *Independent component filters of natural images compared with simple cells in primary visual cortex*, Proc. R. Soc. Lond. B, 265 (1998), pp. 359–366.
[19] W. P. ZIEMER, *Weakly Differentiable Functions*, Springer Verlag, 1989.